

**Paul G. Stankiewicz<sup>1</sup>**

Department of Mechanical and Nuclear Engineering,  
The Pennsylvania State University,  
University Park, PA 16802  
e-mail: pgs5031@gmail.com

**Alexander A. Brown**

Department of Mechanical and Nuclear Engineering,  
The Pennsylvania State University,  
University Park, PA 16802  
e-mail: alexanderallenbrown@gmail.com

**Sean N. Brennan**

Associate Professor  
Mem. ASME  
Department of Mechanical and Nuclear Engineering,  
The Pennsylvania State University,  
University Park, PA 16802  
e-mail: sbrennan@psu.edu

# Preview Horizon Analysis for Vehicle Rollover Prevention Using the Zero-Moment Point

*This research estimates the minimum preview time needed to prevent untripped wheel lift events by analyzing simple maneuvers that are idealizations of a human driver's response in collision avoidance situations. To predict a vehicle's future rollover propensity, the zero-moment point (ZMP) metric is applied to projected vehicle trajectories. Comparing different amounts of preview, the results show that short-range predictions, ranging from 0.1 s to 0.7 s, are sufficient to prevent nearly all dynamics-induced rollovers in typical highway curves. These results are useful to determine the minimum preview horizons, with respect to rollover, that may be necessary for more advanced vehicle control methods, such as model predictive control (MPC). [DOI: 10.1115/1.4030390]*

## 1 Introduction

Over  $5.5 \times 10^6$  crashes were reported by the National Highway Traffic Safety Administration (NHTSA) [1] in the United States in 2009. Almost 31,000 of these crashes were fatal. Vehicle rollover remains one of the deadliest types of automobile accident(s); although rollover occurred in only 2.2% of the total crashes, it accounted for 10.7% of the total fatalities [1]. With increasing focus on driver-assist functionality, modern vehicles are being equipped with the sensors and actuators necessary to detect and eventually mitigate these events.

This research uses the ZMP to predict the onset of future wheel lift over a specified preview time. In particular, the focus of this paper is an analysis of the preview time needed to prevent the onset of untripped rollover. Fixed look-ahead preview methods are a mature concept [2], yet the primary goal of these approaches is generally lane-keeping and collision avoidance, not rollover prevention. The research field is rich with literature on different preview strategies for path following and collision avoidance [3–11]. These strategies range from low complexity metrics that establish time-to-line crossing [3], to higher complexity frameworks based on elastic bands for path planning through stationary and moving traffic [4]. To consider rollover initiation within a predictive horizon, this work is motivated by the increasing use of MPC, wherein dynamics are analyzed over a fixed horizon ahead. Control techniques using MPC are promising in path planning applications due in part to their ability to handle system nonlinearities and trajectory constraints. For example, the work in Refs. [5,6] aims to optimize lane keeping and collision avoidance intervention by computing the smallest possible corrective action needed to keep the driver safe. Similar in nature, the work in Ref. [7] uses MPC algorithms to plan the vehicle's trajectory and establish the minimum threat to the vehicle. Using this threat, the level of intervention is calculated: too much intervention can be seen as intrusive, while too little can result in an accident. MPC is also useful for path planning and collision avoidance in special circumstances, such as when the vehicle is driving on slippery or icy roads [8–10]. Efforts have also been taken to combine haptic

human-machine interaction with MPC-based path planning algorithms [11].

Although not quite as extensive, there has been some research on preview strategies regarding vehicle rollover. One method that attempts to preview roll behavior is the time-to-rollover (TTR) metric [12,13]. Previewed metrics such as the TTR are being extended to heavy-duty vehicle applications for warning systems in emergency maneuvers [14]. Additionally, work on MPC-based rollover prevention limits the peak roll angle by optimally braking each wheel [15] and by combining differential braking with steering intervention [16].

As discussed previously, the dynamics of the system in MPC are analyzed over a fixed horizon ahead. One of the key tuning parameters in MPC formulations is the choice of this preview horizon to ensure sufficient consideration of dynamics such that control actions chosen at the present time step satisfy constraints on system dynamics. However, these horizons with respect to rollover are often determined based on a guess/check methodology. In general, most of the papers above suggest preview horizon times between 0.3 and 2 s as appropriate, but this is a very wide window of uncertainty. The contribution of this paper is to explicitly examine the necessary preview time for simple but representative intervention strategies that may result in untripped rollover.

The remainder of the paper is organized as follows: First, the vehicle models used in this work are introduced and the concepts and equations of the ZMP are further explained in Sec. 2. Section 3 presents the methodology used to preview the dynamic system to gain information about the vehicle states and ZMP in the future. In Sec. 4, simulation procedures and results are then provided to determine the minimum preview time needed to prevent dynamics-induced wheel lift for the given steering intervention. Section 5 provides conclusions that summarize the main contributions of this work.

## 2 Application of ZMP as a Vehicle Rollover Metric

Much of the current research regarding vehicle rollover aims to measure or predict a vehicle's rollover propensity. The most explicit method of determining rollover propensity is full-scale vehicle testing. However, full-scale testing is expensive and incomplete; it is impossible to recreate all possible driving situations when considering the road trajectory, vehicle speed, variations in terrain, weather conditions, and possible obstacles in the road.

Alternatively, research is also being performed to measure rollover propensity by establishing model-based metrics that quantify

<sup>1</sup>Corresponding author.

Contributed by the Dynamic Systems Division of ASME for publication in the JOURNAL OF DYNAMIC SYSTEMS, MEASUREMENT, AND CONTROL. Manuscript received January 29, 2014; final manuscript received March 30, 2015; published online May 29, 2015. Assoc. Editor: Junmin Wang.

the onset of rollover. Several variations of rollover metrics exist including static or steady-state metrics, dynamic metrics, metrics utilizing the knowledge of ground-vehicle forces, and metrics considering the vehicle's states. A commonly used static metric is the static stability factor (SSF) [17]. Dynamic metrics that account for the vehicle's acceleration and inertia include the dynamic stability index [18], while examples based on ground-vehicle forces include the load transfer ratio [19] and the stability moment [20]. Metrics based on vehicle states can also be used for situation-dependent driving to anticipate rollover such as those developed by Carlson and Gerdes [16,21] and the previously mentioned TTR metric proposed by Chen and Peng [12,13].

The metrics presented above are useful but can be limited by their inherent assumptions. Simplified static metrics such as SSF are easy to calculate, but may not provide the accuracy needed to evaluate roll stability during extreme driving scenarios. Dynamic metrics are more suited to transient analysis, but often rely on data that may be difficult to obtain, such as suspension parameters and/or vehicle-ground contact forces. Sensors capable of obtaining suspension or tire forces are expensive and uncommon on typical passenger vehicles. Further, terrain effects on road profiles are also a concern that is often ignored in predicting vehicle rollover.

To address the limitations of the metrics presented above, Lapa-pong [22–26] developed a dynamic rollover metric utilizing the concept of the ZMP. The ZMP is defined as the point on the ground where the summation of the tipping moments acting on an object, due to gravity and inertia forces, equals zero [27]. This concept of using inertial responses rather than force measurements for roll stability analysis was originally developed by Vukobratovic [28] in 1968 and has been applied to maintain the dynamic stability of bipedal robots.

Applying the concept of the ZMP as a vehicle rollover metric presents several advantages. One advantage of the ZMP is that it explicitly accounts for terrain effects in its derivation. Another significant advantage is that calculation of the ZMP does not rely on knowledge of the vehicle-ground contact forces. While the ZMP has proven accurate and useful as a design parameter for rollover indication [26], it has not yet been applied in a predictive manner for ground vehicles. This is the focus of this work.

**2.1 Vehicle Models.** Two vehicle models were considered in this research: the well-known two degrees-of-freedom (2DOF)

rigid model [18] and the three degrees-of-freedom (3DOF) roll model developed by Mammam [29]. The 2DOF rigid model, shown in Fig. 1(a), only considers the vehicle's lateral and yaw dynamics. This model relies on the following assumptions: the vehicle is symmetric along its longitudinal axis, no motion exists in the roll and pitch directions, the vehicle is steered by the front wheel, longitudinal velocity is constant, small angle approximations apply, a linear tire model is applied, all components of the model are rigid, the tires roll without slip in the longitudinal direction, and aerodynamic effects are negligible.

The 3DOF roll model, shown in Fig. 1(b), considers lateral, yaw, and roll dynamics, where a sprung mass of the vehicle rotates about the roll center of an unsprung rigid mass. This model relies on many of the same assumptions as the 2DOF rigid model, along with the following additional assumptions: a sprung mass sits atop the unsprung mass and both are connected via a torsional spring and torsional damper, the spring and damper are linear, the roll center is fixed with respect to the vehicle's body, and the unsprung mass only rotates in the yaw direction. Shim and Ghike explore the appropriateness of model assumptions when analyzing roll dynamics in Ref. [30]. Full derivations for both models used in this study are provided in Ref. [24]. While the roll model considers the vehicle's suspension dynamics as an additional DOF, both models are subject to the same lateral and yaw dynamics. A free-body diagram illustrating the lateral and yaw dynamics for both models is shown in Fig. 2. The body-fixed coordinate system developed by the Society of Automotive Engineers (SAE) [31] was used to derive both models. Parameters used in the vehicle models are provided in Table 1.

**2.2 Inclusion of Terrain Effects in Vehicle Models.** For drainage or for sharp curves, public road profiles are generally not level in the lateral direction. This is also the case just outside the road boundaries, as the shoulder and median of a road typically slope away from the pavement. Therefore, it is necessary to take the road bank angle (superelevation) into consideration for both on-road and road departure driving situations. To maintain a linear system, the terrain angle,  $\phi_t$ , is treated as an exogenous linear input to the system dynamics such that the state-space representations of the vehicle models now have two inputs: steering angle and terrain bank angle. Although the terrain cannot be controlled, it can be treated as a known input by utilizing mapped information

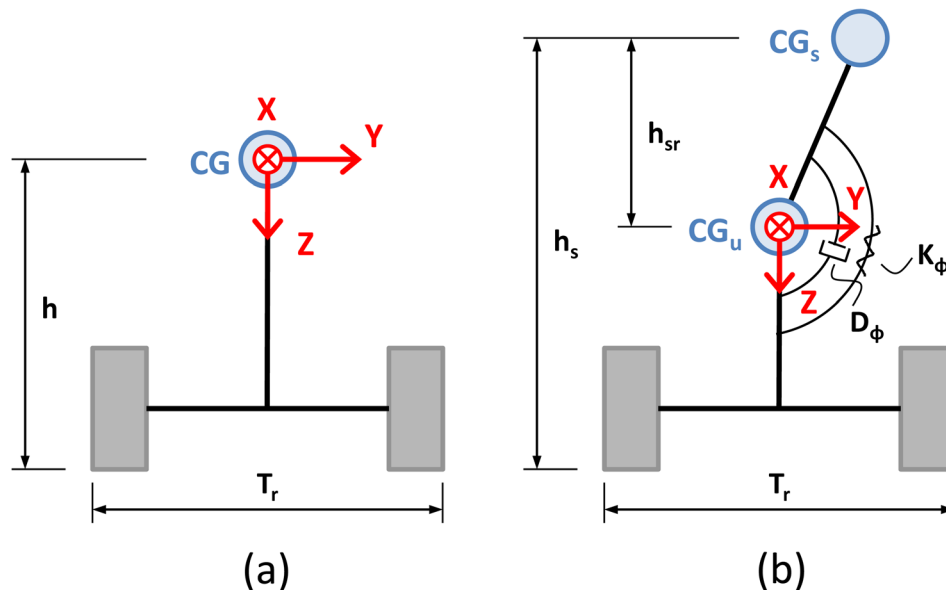
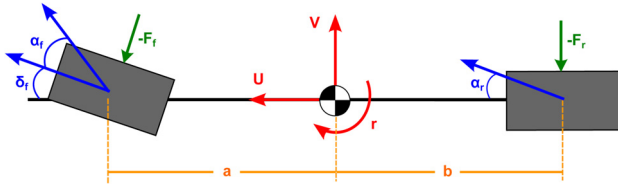


Fig. 1 Vehicle models viewed along the body-fixed  $x$ -axis for (a) 2DOF rigid model (b) 3DOF roll model. CG refers to the rigid model's center-of-gravity for the total mass.  $CG_u$  and  $CG_s$ , meanwhile, refer to the unsprung mass and sprung mass, respectively, of the roll model.



**Fig. 2 Free-body diagram illustrating the vehicle's lateral and yaw dynamics**

**Table 1 Parameters for vehicle models and ZMP**

Symbol	Definition
$U$	Longitudinal velocity of CG/CG <sub>u</sub> (body-fixed)
$y$	Lateral position of CG/CG <sub>u</sub> (body-fixed)
$V$	Lateral velocity of CG/CG <sub>u</sub> (body-fixed)
$a_G$	Lateral acceleration of CG/CG <sub>u</sub> (body-fixed) <sup>a</sup>
$\phi_r$	Roll angle
$\theta$	Pitch angle
$\psi$	Yaw angle
$r$	Yaw rate
$m$	Total vehicle mass
$m_s$	Sprung vehicle mass
$L$	Length of vehicle
$T_r$	Track width of vehicle
$a$	CG/CG <sub>u</sub> to front axle distance
$b$	CG/CG <sub>u</sub> to rear axle distance
$I_{xx}$	Mass moment of inertia about vehicle $x$ -axis <sup>a</sup>
$I_{xz}$	Product mass moment of inertia <sup>a</sup>
$h_{sr}$	Height of sprung mass from roll center
$h$	Height of vehicle
$C_{zf}$	Front cornering stiffness
$C_{zr}$	Rear cornering stiffness
$\alpha$	Tire slip angle
$\delta_r$	Front steering angle
$\phi_t$	Terrain superelevation
$K_\phi$	Roll stiffness
$D_\phi$	Roll damping constant
$g$	Gravitational acceleration

<sup>a</sup>Subscripts  $x$ ,  $y$ , and  $z$  indicate  $x$ -,  $y$ -, and  $z$ -directions, respectively.

about the vehicle's surroundings. Mapped information allows the vehicle to localize itself using visible subsets of a global frame [32], and thus can aid in real-time perception by linking features, such as terrain variations, with Global Positioning System (GPS) locations. The terrain bank angle is assumed to remain constant throughout this paper; however, variations in profile, if they are known, can readily be included. The full derivation of terrain input in the vehicle model is presented in Ref. [24].

**2.3 Calculation of ZMP.** As discussed previously, the ZMP is defined as the point on the ground where the summation of the tipping moments acting on an object, due to gravity and inertia forces, equals zero [27]. By treating the vehicle as a kinematic chain, it is possible to calculate each body's net moment contribution to the ZMP. This calculation only requires measurement of the kinematic motion of all objects in the chain, information that is accessible through inertial measurement units and knowledge of the vehicle parameters. If a vehicle's ZMP moves outside the vehicle's support polygon, the vehicle will begin to overturn. Although the location of the ZMP exists in three-dimensional space, only the coordinate of its lateral position on the ground from the vehicle centerline, called  $y_{ZMP}$ , is necessary for the application to vehicle rollover [24]. This is because, for conventional vehicles, the occurrence of wheel lift about the vehicle's pitch axis is extremely rare compared to wheel lift about the vehicle's roll axis. In a vehicle, the boundaries of the contact polygon are

defined where the four tires touch the ground. The distance of  $y_{ZMP}$  from the centroid of the contact polygon is used as the metric for the vehicle's rollover propensity. More specifically, if  $y_{ZMP}$  is located outside the track width of the vehicle, wheel lift will occur [24].

Lapapong [24] derived the location of the ZMP for both the 2DOF rigid model and the 3DOF roll model. The results showed that  $y_{ZMP}$  was nearly identical for both vehicle models when applied to a real vehicle. Therefore, only the result of the simpler  $y_{ZMP}$  calculation for the 2DOF rigid model is presented. Parameters used in the  $y_{ZMP}$  calculation are provided in Table 1. The location of  $y_{ZMP}$  for the rigid model can be expressed as

$$y_{ZMP} = \{mg \cos(\theta) \sin(\phi_r) [T_r |\tan(\phi_r - \phi_t)| + 2h] - ma_{Gy} [T_r |\tan(\phi_r - \phi_t)| + 2h] - 2I_{xx} \ddot{\phi}_r + 2I_{xz} \dot{r} + 2I_{yz} (\dot{\theta}^2 - r^2) + 2(I_{xz} + I_{yy} - I_{zz}) \dot{\theta} r\} / \{2m [g \cos(\theta) \cos(\phi_t) \sec(\phi_r - \phi_t) - a_{Gy} \tan(\phi_r - \phi_t) - a_{Gz}]\} \quad (1)$$

Because the  $y_{ZMP}$  equation can be applied interchangeably between the two vehicle models, the simpler form of the  $y_{ZMP}$  equation given in Eq. (1) is applied to the roll model for this study, as shown in Fig. 3. A simplified linear equation of Eq. (1), found in Ref. [26], is expressed as

$$y_{ZMP} = -\frac{I_{xx}}{mg} (\ddot{\phi}_t + \ddot{\phi}_r) + h_{sr} (\phi_t + \phi_r) - \frac{h_{sr}}{g} a_{Gy} \quad (2)$$

Equation (2) is merely a linear combination of vehicle states. Indeed, this is a state combination used in other roll research [33].

The ZMP location can readily be added as an output of a state-space model of a vehicle inclusive of roll, for example, the 3DOF model discussed earlier. Assuming the state vector used for the roll model is given as

$$x = [y \quad V \quad r \quad \dot{\phi}_r \quad \phi_r \quad \psi]^T \quad (3)$$

and recognizing the general state-space notation of

$$\dot{x} = Ax + Bu \quad (4)$$

where  $u$  is the input vector to the system (steering angle and terrain bank angle), the  $A$  and  $B$  matrices are obtained from

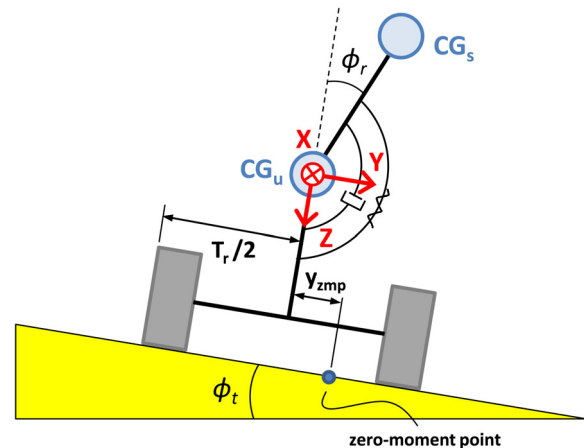


**Fig. 3 Roll model on banked slope with zero moment point illustration**

$$M_{\text{int}} = \begin{bmatrix} m & 0 & m_s h_{\text{sr}} & 0 \\ m_s h_{\text{sr}} & -I_{xz} & (I_{xx} + m_s h_{\text{sr}}^2) & 0 \\ 0 & I_{zz} & -I_{xz} & 0 \\ 0 & 0 & 0 & 1 \end{bmatrix} \quad (5)$$

$$N_{\text{int}} = \begin{bmatrix} \frac{-C_{zf} - C_{zr}}{U} \left( mU + \frac{bC_{zr} - aC_{zf}}{U} \right) & 0 & 0 & 0 \\ 0 & m_s h_{\text{sr}} U & D_\phi & (K_\phi - m_s h_{\text{sr}} g) \\ \frac{bC_{zr} - aC_{zf}}{U} & \frac{-a^2 C_{zf} - b^2 C_{zr}}{U} & 0 & 0 \\ 0 & 0 & -1 & 0 \end{bmatrix} \quad (6)$$

$$F_{\text{int}} = \begin{bmatrix} -C_{zf} & mg \\ 0 & m_s h_{\text{sr}} g \\ -aC_{zf} & 0 \\ 0 & 0 \end{bmatrix} \quad (7)$$

$$A_{\text{int}} = -M_{\text{int}}^{-1} N_{\text{int}} \quad (8)$$

$$B_{\text{int}} = M_{\text{int}}^{-1} F_{\text{int}} \quad (9)$$

such that

$$A = \begin{bmatrix} 0 & [1 & 0 & 0 & 0] & U \\ 0_{4 \times 1} & [A_{\text{int}}] & 0_{4 \times 1} \\ 0 & [0 & 1 & 0 & 0] & 0 \end{bmatrix} \quad (10)$$

$$B = \begin{bmatrix} 0_{1 \times 2} \\ [B_{\text{int}}] \\ 0_{1 \times 2} \end{bmatrix} \quad (11)$$

The roll acceleration and lateral acceleration can be written in terms of the  $A$  and  $B$  matrices of the roll model in the form

$$\ddot{\phi}_r = [0 \ 0 \ 0 \ 1 \ 0 \ 0][Ax + Bu] \quad (12)$$

$$a_{Gy} = [0 \ 1 \ 0 \ 0 \ 0 \ 0][Ax + Bu] + Ur \quad (13)$$

Equation (2) can then be written in terms of the  $A$  and  $B$  matrices of the roll model in the form

$$y_{\text{ZMP}} = \begin{bmatrix} 0 & -\frac{h_{\text{sr}}}{g} & 0 & -\frac{I_{xx}}{mg} & 0 & 0 \end{bmatrix} [Ax + Bu] + h_{\text{sr}} \left( \phi_t + \phi_r - \frac{Ur}{g} \right) \quad (14)$$

where  $\ddot{\phi}_t = 0$  due to the assumption that the terrain bank angle is constant.

Equation (14) is capable of calculating the vehicle's rollover propensity at the current time. However, to prevent a rollover event through pre-emptive action, it is necessary to predict the vehicle's rollover propensity over a preview horizon based on the current states and inputs.

### 3 Fixed Point Preview of Dynamic Vehicle Model

**3.1 Generalized Preview Solution of a Dynamic System.** The methodology for previewing the state-space model will now be introduced. Previewed information can be obtained by extending the current states and inputs of the system over a specified preview interval, assuming a known control input. Considering the following linear system

$$\begin{aligned} \dot{x} &= Ax(t) + Bu(t) \\ y &= Cx(t) + Du(t) \end{aligned} \quad (15)$$

the general solution is given by

$$x(t+T) = \Phi(t+T, t)x(t) + \int_t^{t+T} \Phi(t+T, \tau)B(\tau)u(\tau)d\tau \quad (16)$$

where  $T$  is the preview time and  $\Phi$  is the system's state transition matrix [34]. The state transition matrix is determined by the Peano-Baker series, which for a linear time-invariant system, reduces to the matrix exponential in the form

$$\Phi(t+T, t) = \sum_{k=0}^{\infty} \frac{A^k T^k}{k!} = e^{AT} \quad (17)$$

The solution given by Eq. (16) allows the calculation of the state vector at time  $t+T$  using the current state vector and the input during the preview time. To utilize this solution, several approximations of the state transition matrix exist, for example, Euler, bilinear (Tustin), and numerical approximations. Each of these approximations was considered in the research. Numerical approximation of the state transition matrix is achieved by directly calculating the matrix exponential within MATLAB. Preliminary simulations showed that MATLAB's numerical approximation of the state transition matrix, Eq. (17), provided the most accurate results. This approximation is used for the rest of the paper, hereafter referred to as the preview  $A$  matrix,  $A_p$ , introduced in Sec. 3.2.

**3.2 Application of Previewed Information to Vehicle Rollover.** The general solution given by Eq. (16) can be applied to the vehicle rollover problem. For this application, the desired output of the system is the previewed value of  $y_{\text{ZMP}}$ , termed  $y_{\text{ZMP}}(t+T)$ , which can be obtained by selecting the appropriate  $C$  and  $D$  output matrices in the state-space model. Assuming that the  $A$  and  $B$  matrices are time-invariant and utilizing the assumption that the steering input and terrain bank angle remain constant over the (short) preview interval, the general solution of Eq. (16) for the previewed state vector can be simplified. For the case in which only the state vector at time  $t+T$  is desired, Eq. (16) simplifies to the following:

$$x(t+T) = \Phi(t+T, t)x(t) + \Psi T B u \quad (18)$$

where  $u$  is the constant system input and

$$\Psi = I + \sum_{k=1}^{\infty} \frac{(TA)^k}{(k+1)!} \quad (19)$$

Using Eq. (18) and the state transition matrix approximation discussed previously, one can obtain a previewed state vector and thereby calculate a previewed ZMP estimate. The previewed numerical approximation of the input term is hereafter referred to as the preview  $B$  matrix,  $B_p$ , such that

$$A_p = \Phi_{\text{num}}(t+T, t) \quad (20)$$

$$B_p = \Psi T B \quad (21)$$

and Eq. (18) is written as

$$x(t+T) = A_p x(t) + B_p u(t) \quad (22)$$

Now that the previewed state vector is defined, the ZMP as defined in Eq. (14) can be predicted at a future time. Roll acceleration at the preview time is given by

$$\ddot{\phi}_r(t+T) = [0 \ 0 \ 0 \ 1 \ 0 \ 0][Ax(t+T) + Bu(t+T)] \quad (23)$$

Again, it is recognized that all inputs are assumed constant over the preview interval such that  $u(t+T) = u(t)$ . This means that for the predictive state calculation, the inputs to the system at the current time step are assumed to remain constant up to the preview time. Then, substituting Eq. (22) gives the future roll acceleration based on the present states and inputs

$$\ddot{\phi}_r(t+T) = [0 \ 0 \ 0 \ 1 \ 0 \ 0][A[A_p x + B_p u] + Bu] \quad (24)$$

The previewed roll angle and previewed lateral acceleration can also be simplified in this manner resulting in the following equation for  $y_{ZMP}$  at the preview time:

$$y_{ZMP}(t+T) = \begin{bmatrix} 0 & -\frac{h_{sr}}{g} & 0 & -\frac{I_{xx}}{mg} & 0 & 0 \end{bmatrix} [A[A_p x + B_p u] + Bu] + \begin{bmatrix} 0 & 0 & -\frac{h_{sr}U}{g} & 0 & h_{sr} & 0 \end{bmatrix} [A_p x + B_p u] + h_{sr}\phi_t \quad (25)$$

Equation (25) can be used to add the previewed  $y_{ZMP}$  at time  $t+T$  as an output of the state-space vehicle model at time  $t$ .

#### 4 Rollover Prevention Using Previewed ZMP

An important application of previewed  $y_{ZMP}$  could be to detect when a driver's present steering input will soon result in wheel lift. By identifying impending rollover in the near future, present steering actions or warnings can be given to potentially correct the steering input to mitigate the risk. For implementation of this approach, it is necessary to determine the minimum preview time needed to predict and prevent a rollover event. Insufficient preview does not provide enough advanced warning to mitigate the risk, whereas too much preview degrades the accuracy of the predictive state calculations. This section examines the use of previewed  $y_{ZMP}$  to determine the minimum necessary preview time to prevent rollover.

A "worst-case" driving situation as defined in Ref. [26] was considered for the MATLAB simulation in order to maximize the vehicle's rollover propensity. The parameters for a 1989 GMC 2500 pick-up truck, shown in Table 2, were used due to the vehicle's high center-of-gravity. A highway speed of 26.8 m/s (60 mph) was used, as well as the introduction of an 8 deg bank angle (14% superelevation), a value representative of the designed bank angle in a sharp highway curve [35]. The steering input was designed so that the vehicle turns up the slope of the terrain. This driving scenario is not uncommon; a vehicle that travels onto the

Table 2 Parameters for 1989 GMC 2500 pick-up truck

Symbol	Value	Unit
$m$	3255	kg
$m_s$	2956	kg
$a$	1.895	m
$b$	1.459	m
$h$	1.234	m
$h_{sr}$	0.781	m
$C_{zf}$	-120,000	N/rad
$C_{zr}$	-120,000	N/rad
$T_r$	1.615	m
$I_{xx}$	1830	kg/m <sup>2</sup>
$I_{yy}$	6488	kg/m <sup>2</sup>
$I_{zz}$	7913	kg/m <sup>2</sup>
$I_{xz}$	500	kg/m <sup>2</sup>
$D_\phi$	4500	N m s/rad
$K_\phi$	145,330	N m/rad
$g$	9.81	m/s <sup>2</sup>

shoulder or median of a highway would experience similar circumstances and a similar steering input as the driver tries to correct his/her path. It should be noted that the following results would likely change for different vehicle configurations, speeds, environments, and intervention strategies. However, the process of determining the minimum preview time would remain the same such that these variables could be readily modified for the particular scenario being tested.

**4.1 Corrective Steering Maneuver #1.** Because advanced closed-loop control laws for wheel-lift prevention, such as MPC approaches, can be computationally intensive and sensitive to algorithm architecture and tuning, this study examines the effects of corrective steering maneuvers on the preview horizon using open-loop analysis. This is specifically advantageous as it limits the coupling between a feedback algorithm and  $y_{ZMP}$ , eliminating the need for a receding horizon approach that requires recalculation of optimal steering maneuvers at each time step. The simplicity of an open-loop analysis allows for a thorough development of the methodology for determining the safe maneuver envelope of the vehicle without narrowing the analysis to a particular corrective steering law. This way, the results that follow can be trivially extended with the addition of other corrective inputs, such as braking, or extended for use in the design of closed-loop intervention strategies like MPC. It should also be noted that the following open-loop steering actions are not considered optimal intervention strategies and are not suggested to be implemented in practice. Rather, these maneuvers are simply meant to represent the gross behavior of a hypothetical driver in an emergency scenario and subsequently examine their effect on the preview horizon necessary to prevent wheel lift.

In this study, the initial driver steering input of the tires is chosen to follow a simple sinusoidal trajectory to the desired steering amplitude and then remain constant. This is meant to approximate a driver performing an evasive maneuver by rapidly steering away from his/her current path. The proposed initial steering of the driver then takes the form

$$\delta_f = \begin{cases} \frac{A}{2} \sin\left(2\pi ft - \frac{\pi}{2}\right) + \frac{A}{2} & \text{for } 0 < t \leq \frac{1}{2f} \\ A & \text{for } t > \frac{1}{2f} \end{cases} \quad (26)$$

where  $A$  is the steering angle amplitude of the tires, and  $f$  is the steering frequency (Hz).

The wheel lift prevention control considered here is simple as well and open-loop in nature. If the system detects that previewed  $y_{ZMP}$  has gone outside the vehicle's track width (indicating future wheel lift), it will implement a corrective steering input in which the steering angle of the tires follows a sinusoidal correction (of the same frequency) from its current value back to a zero steering input in the form

$$\delta_f = \begin{cases} \frac{A}{2} \sin\left(2\pi ft + \frac{\pi}{2}\right) + \frac{A}{2} & \text{for } t^* < t \leq t^* + \frac{1}{2f} \\ 0 & \text{for } t > t^* + \frac{1}{2f} \end{cases} \quad (27)$$

where  $T_r$  is the track width of the vehicle and the sign of  $A$  is consistent with the initial driver steering input. The reader should note that Eq. (27) is not meant to be a general control law; it is simply a mathematical description of how the open-loop steering correction was implemented for this study.

Figure 4 illustrates corrective steering maneuver #1, described by Eqs. (26) and (27), in graphical form. The axes of Fig. 4 have purposefully been generalized for any value of steering angle and

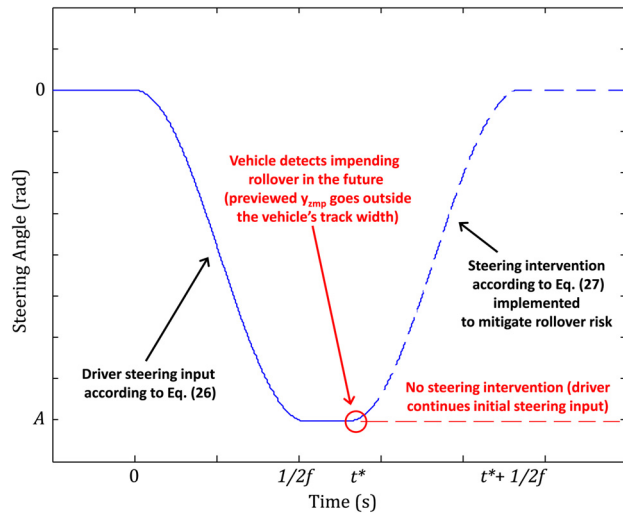


**Fig. 4 Generalized example of corrective steering maneuver #1 simulations**

steering frequency. This is because this study aims to investigate how the severity of the driver's initial steering input affects the necessary preview time for a successful intervention in the form of wheel lift prevention. Therefore, combinations of steering angle and steering frequency were considered to determine the necessary preview time to prevent wheel lift. Simulations of the steering scenario were performed for each combination of steering angle and steering frequency. These steering values cover the effective range imposed by limits on the steering rack. It is also assumed that there is no tire skidding for the given maneuvers. Previous work by the authors [26] showed that wheel lift will occur before the tires skid for steering frequencies below 0.8 Hz. Therefore, results for steering frequencies above this value should be considered questionable as skidding is likely to precede rollover.

Using the linear model presented earlier,  $y_{ZMP}$  and  $y_{ZMP}(t+T)$  were calculated throughout the simulations to evaluate the vehicle's roll stability. For this study,  $y_{ZMP}$  has been normalized by the track width of the vehicle such that values greater than one or less than  $-1$  represent wheel lift. The minimum acceptable preview time was determined as follows: for each combination of steering angle and steering frequency, the preview time was iteratively increased from zero by 0.01 s until the peak value of the normalized current (real-time, as opposed to previewed)  $y_{ZMP}$  fell between 0.97 and 0.98 (or  $-0.97$  and  $-0.98$ ). At this point, wheel lift prevention was considered to have occurred and the preview time was recorded. An illustrative example of this process is shown in Fig. 5 for one specific combination of steering amplitude and steering frequency,  $-8.5$  deg and 0.55 Hz, respectively. This figure shows how the peak value of the real-time  $y_{ZMP}$  decreases as the preview time is increased. For this steering combination, the minimum preview time to prevent wheel lift using the process described above is 0.33 s, where the peak value of real-time  $y_{ZMP}$  drops below 0.98.

The multibody simulation software CARSIM was also used to assess the fidelity of the results obtained using the linear system. CARSIM ensures that the significant assumptions used in the formulation of the previewed linear system remain appropriate when considering the complex nonlinearities expected during such maneuvers, such as changes in the tire and suspension properties due to load transfer and rapid steering. These nonlinear effects are fitted to the CARSIM model with the basic vehicle parameters used for the 3DOF model. In CARSIM, the preview time associated with a wheel lift event was recorded when the vertical force of any tire fell between 200 N and 300 N (range of 2–3% of the static load on each tire), a value low enough to indicate that wheel lift is imminent.

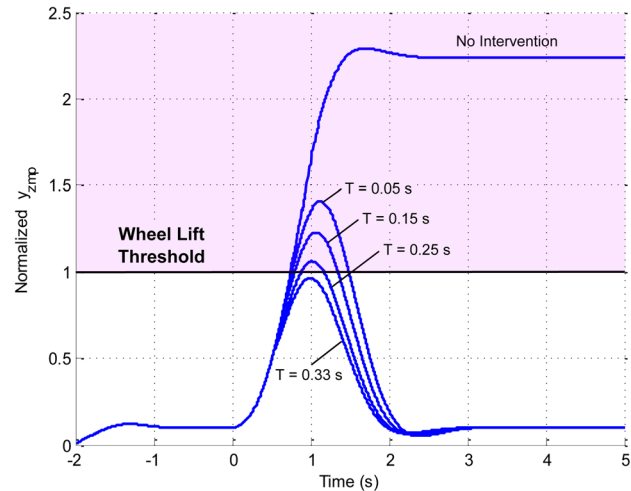


**Fig. 5 Example of the iterative calculation of the preview time for corrective steering #1**

The simulation outputs of  $y_{ZMP}$  and  $y_{ZMP}(t+T)$  for the same combination of steering amplitude and steering frequency,  $-8.5$  deg and 0.55 Hz, respectively, are shown in Fig. 6. The iterative structure described previously was used to calculate the preview time for this steering combination, i.e., when the normalized value of current  $y_{ZMP}$  fell between its prescribed limits of 0.97 and 0.98. For the plot shown in Fig. 6(a), the minimum necessary preview time was found to be 0.33 s, as shown in Fig. 5. Thus, shorter preview times than this resulted in a normalized peak value of current  $y_{ZMP}$  greater than 0.98, while longer preview times resulted in a peak value less than 0.97. These plots include the  $y_{ZMP}$  calculations for both the linear system and for CARSIM. Specifically, Fig. 6(a) illustrates how the intervention strategy of Eq. (27), implemented when the value of  $y_{ZMP}(t+T)$  rises above the wheel lift threshold, is able to keep the value of current  $y_{ZMP}$  below the wheel lift threshold. Figure 6(b), however, illustrates the same driver input when the intervention strategy of Eq. (27) is not applied. Clearly, when the corrective steering is not applied, the value of real-time  $y_{ZMP}$  rises well above the wheel lift threshold. Therefore, these results show that previewed  $y_{ZMP}$  information is capable of preventing the onset of wheel lift. There is also very good agreement between the linear model and CARSIM calculations of  $y_{ZMP}$  and  $y_{ZMP}(t+T)$ . Comparing the curves between these two models, it can be seen that the roll model calculation is slightly more conservative, as indicated by the higher peak values shown in Fig. 6(a).

The simulations illustrated in Fig. 6 were then repeated for many additional combinations of steering amplitude and steering frequency. The same methods described above were used to determine the minimum necessary preview time. Figure 7 shows how the necessary preview time is affected by the driver's initial steering magnitude and frequency. The information in Fig. 7 is also portrayed in Fig. 8 in the form of a contour plot of the minimum preview times over the range of steering inputs. These plots indicate that the minimum necessary preview time is greatly influenced by the frequency of the steering input (higher frequency means a more severe steering input). As the frequency is decreased, longer preview times are needed to detect and effectively mitigate the wheel lift risk. This relationship can be explained from the Bode plot between the current  $y_{ZMP}$  and steering angle and the Bode plot between previewed  $y_{ZMP}$  and steering angle, shown in Fig. 9. The Bode plot shown in Fig. 9 was calculated by simply performing the frequency response from input to output (rather than state) for the modified  $C$  and  $D$  matrices inclusive of Eqs. (14) and (25). The frequency response of current  $y_{ZMP}$  exhibits a notch filter effect for higher frequencies, while the frequency response of previewed  $y_{ZMP}$  remains relatively

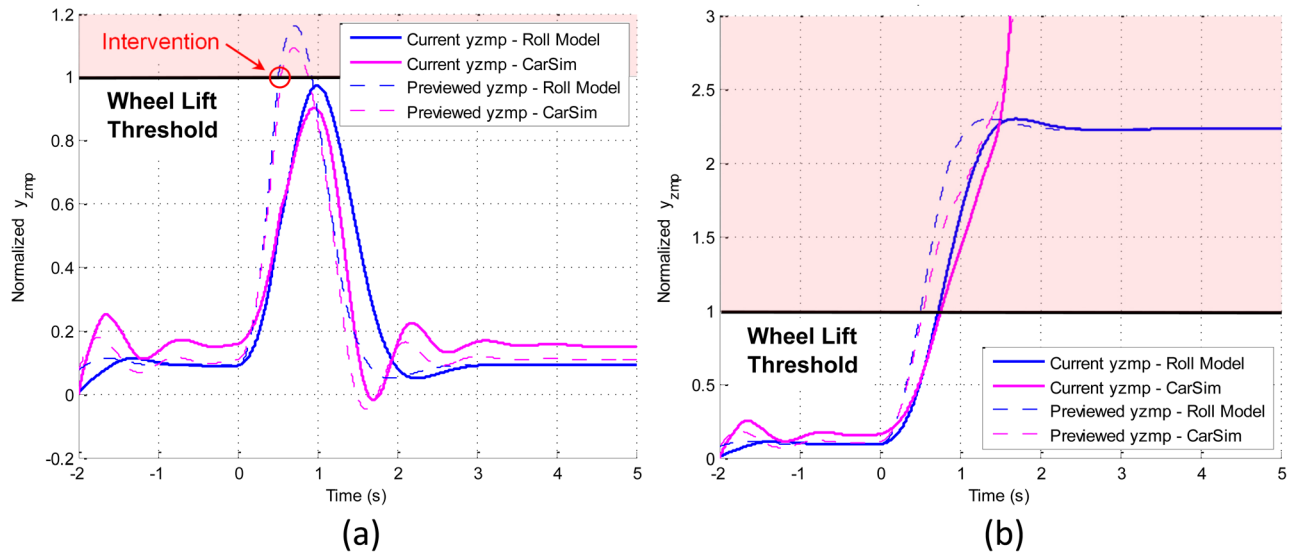


Fig. 6  $y_{ZMP}$  (a) with and (b) without corrective steering #1

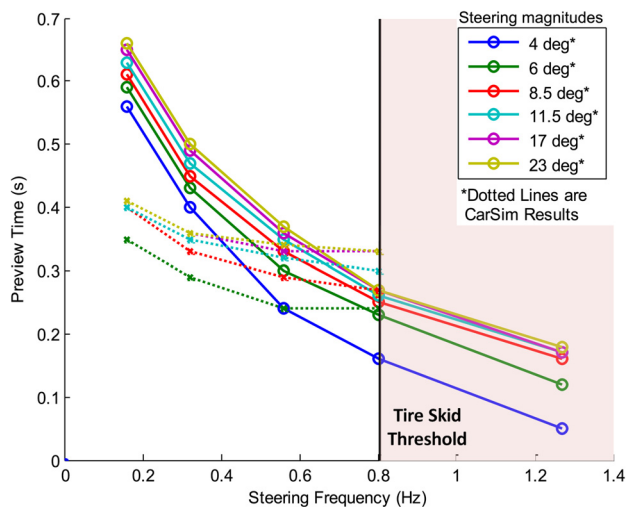


Fig. 7 Minimum preview times needed to prevent wheel lift for corrective steering #1. The “Tire Skid Threshold” indicates the steering frequencies above which skidding is likely to precede rollover.

constant. Thus, since the previewed  $y_{ZMP}$  calculation assumes the steering input at the current time step to be constant over the preview horizon, more severe steering inputs will result in earlier detection and correction through a previewed  $y_{ZMP}$  value that rises quickly compared to the real-time value of  $y_{ZMP}$ . This is due to the higher gain difference between previewed and current  $y_{ZMP}$  in the frequency response at higher frequencies. Impending wheel lift from a less severe steering input (lower frequency), however, will not be detected as quickly and requires more preview to correct the action. This is because the values of current and previewed  $y_{ZMP}$  have the same direct current and low-frequency gain characteristics and rise with approximately the same slope.

The opposite trend is true for changes in steering magnitude: longer preview times are needed as the steering magnitude is increased. Thus, the longest preview time needed for the steering combinations tested was for a low frequency, high magnitude steering input. In Fig. 7, this is a preview time of 0.66 s for a  $-23$  deg, 0.16 Hz steering input. The *CARSIM* results for each steering combination, shown by the dotted lines in Figs. 7 and 8(b), require less preview at frequencies below approximately 0.7 Hz

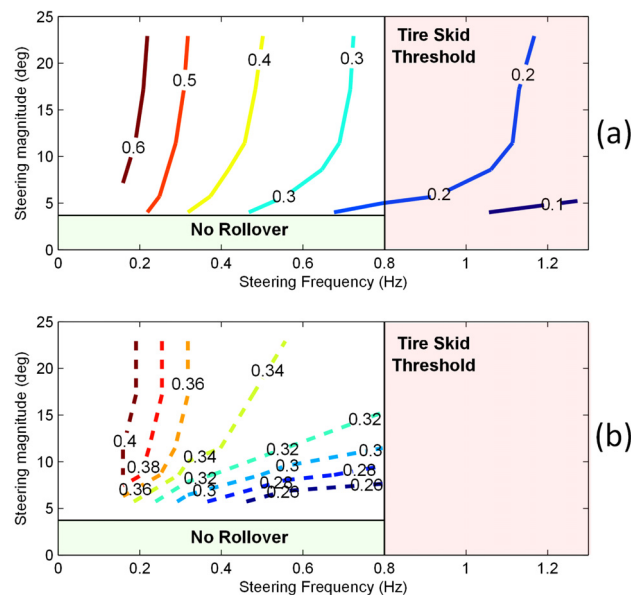


Fig. 8 Contour plots of minimum preview times (s) needed to prevent wheel lift for corrective steering #1 for (a) linear roll model and (b) *CARSIM*. The Tire Skid Threshold indicates the steering frequencies above which skidding is likely to precede rollover. The “No Rollover” zone indicates where steering combinations did not induce wheel lift.

and more preview above this frequency when compared to the linear roll model. This could be due to the tire nonlinearities and dynamics present in *CARSIM*, but not accounted for in the linear model.

**4.2 Corrective Steering Maneuver #2.** A second scenario with a more severe corrective steering input was also simulated. This scenario was designed to more closely resemble the NHTSA Fishhook maneuver prescribed for rollover testing where the vehicle is given an initial rapid steering input followed by an over-correction [36]. However, the steering intervention considered in this section also has applications if the driver wants to stay in his/her original direction of travel but with an offset. Corrective steering maneuver #1 is basically a change in orientation of the vehicle

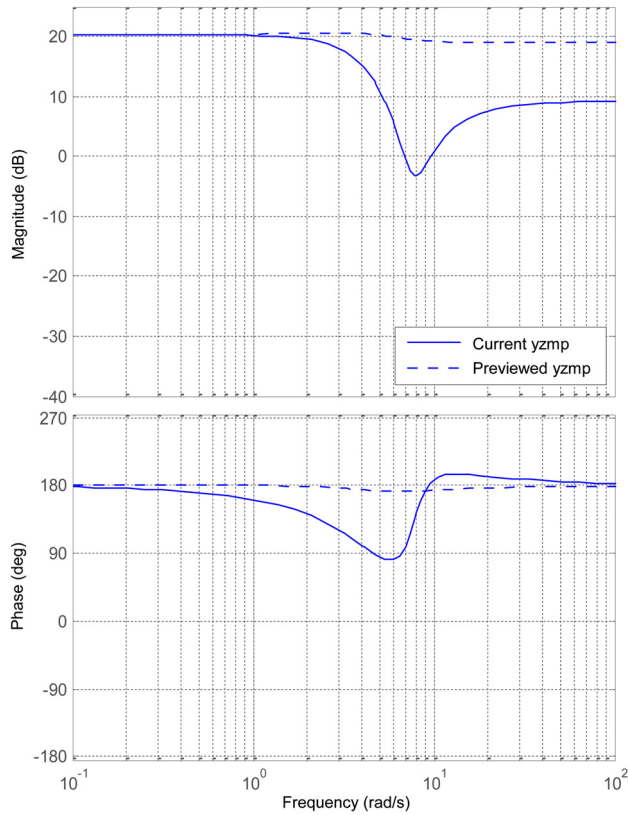


Fig. 9 Bode plot of steering angle and  $y_{ZMP}$

away from its original direction of travel. To remain on the original direction of travel but with an offset, the vehicle must steer back to the travel direction. This can result in over-steering and wheel lift initiation in the corrective portion. Thus, we consider a second case where the steering input consists of both a course departure and a course correction.

All conditions and parameters remain the same, but the corrective steering input now follows a sinusoidal correction to the opposite steering amplitude (over-correction; Eq. (28a)) once impending rollover is detected in the initial driver steering input. Because this over-correction of the steering input opens up the possibility of the vehicle experiencing wheel lift on its opposite side, if the vehicle detects impending rollover during the over-correction, it will implement a second corrective steering input back to zero (Eq. (28b)) in the form

$$\text{if } |y_{ZMP}(t+T)| \geq \frac{T_r}{2} \text{ at } t = t^* \\ \delta_f = \begin{cases} A \sin\left(2\pi ft + \frac{\pi}{2}\right) & \text{for } t^* < t \leq t^* + \frac{1}{2f} \\ -A & \text{for } t > t^* + \frac{1}{2f} \end{cases} \quad (28a)$$

$$\text{if } |y_{ZMP}(t+T)| \geq \frac{T_r}{2} \text{ at } t = t^{**} \\ \delta_f = \begin{cases} -\frac{A}{2} \sin\left(2\pi ft + \frac{\pi}{2}\right) - \frac{A}{2} & \text{for } t^{**} < t \leq t^{**} + \frac{1}{2f} \\ 0 & \text{for } t > t^{**} + \frac{1}{2f} \end{cases} \quad (28b)$$

This open-loop steering trajectory, specified by Eqs. (26) and (28), now mimics a driver that is aggressively steering to both avoid an obstacle and remain in the original direction of travel. Once again, this framework is not meant to produce an optimal

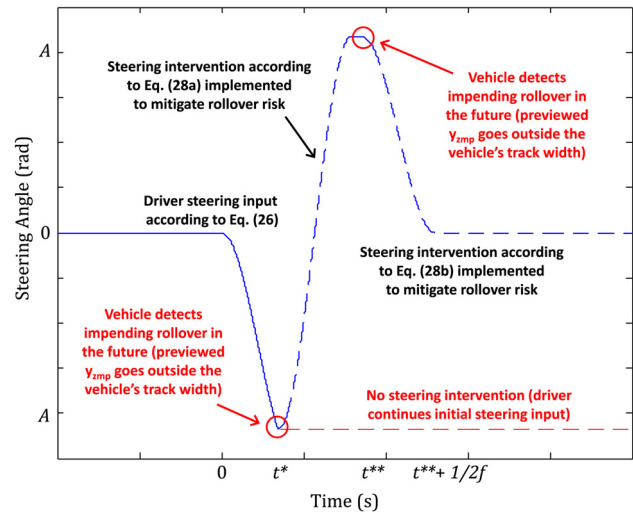


Fig. 10 Generalized example of corrective steering maneuver #2 simulations

control law, but instead to create repeatable driver behavior used to analyze the necessary preview horizon. Similar to Fig. 4, Fig. 10 illustrates corrective steering maneuver #2, described by Eqs. (26) and (28), in graphical form. Again, the axes of Fig. 10 have purposefully been generalized for any value of steering angle and steering frequency.

The simulation outputs of  $y_{ZMP}$  and  $y_{ZMP}(t+T)$  for the same steering combination as Figs. 5 and 6 ( $-8.5$  deg and  $0.55$  Hz) were repeated for this new steering intervention. The procedure for determining the minimum necessary preview time remains the same and is illustrated in Fig. 11. Here, it should be noted that the choice of preview time must keep the value of  $y_{ZMP}$  between the wheel lift thresholds on both sides of the vehicle. Again, the simulation outputs are shown in Fig. 12, where it can be seen in Fig. 12(a) that corrective steering maneuver #2 is able to prevent wheel lift for both the initial driver steering input and the subsequent over-correction. Figure 12(b) illustrates how the value of current  $y_{ZMP}$  drops below the wheel lift threshold for the same maneuver. In other words, wheel lift would occur if the over-correction is not corrected.

Once again, additional combinations of steering amplitude and frequency were simulated to determine the minimum acceptable preview time to prevent wheel lift for corrective steering maneuver #2. These preview times were determined using the same

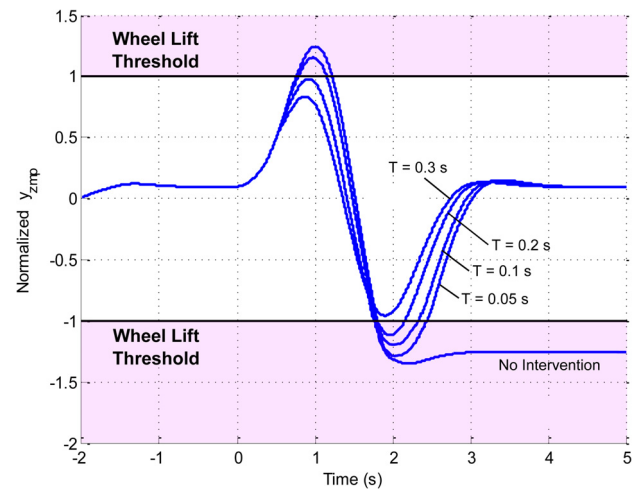


Fig. 11 Example of the iterative calculation of the preview time for corrective steering #2

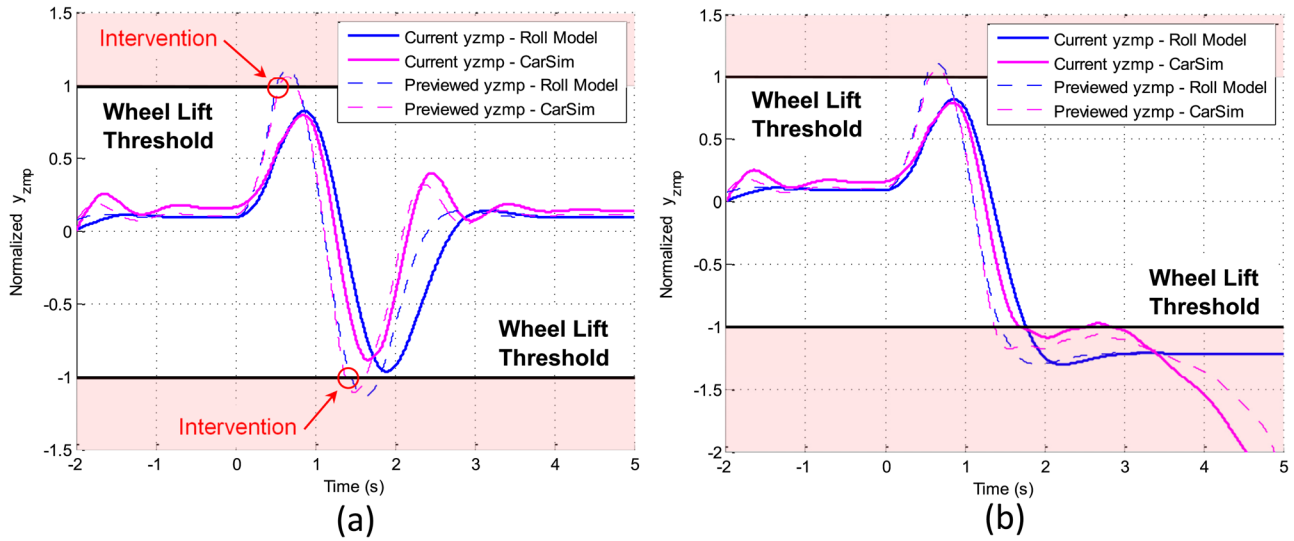


Fig. 12  $y_{zmp}$  (a) with and (b) without corrective steering #2

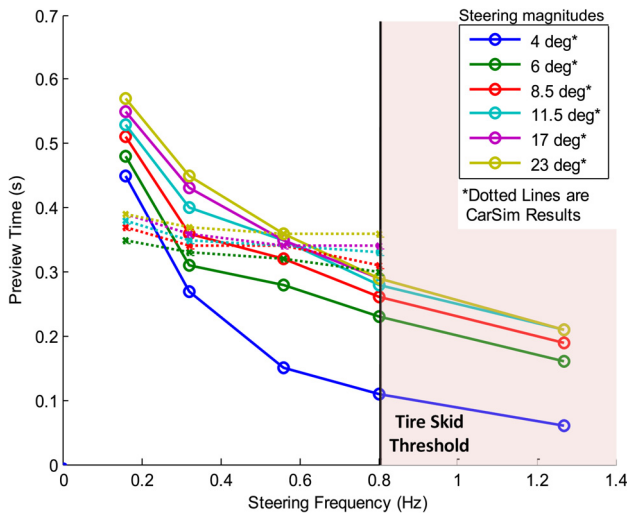


Fig. 13 Minimum preview times needed to prevent wheel lift for corrective steering #2. The Tire Skid Threshold indicates the steering frequencies above which skidding is likely to precede rollover.

procedure as the previous scenario and are presented in Fig. 13 and as a contour plot in Fig. 14. The necessary preview time experiences the same trends as those seen in the analysis of corrective steering maneuver #1. When comparing the necessary preview times between the two steering interventions, it can be seen that slightly less preview time, approximately 0.1 s, is required for the roll model predictions of corrective steering maneuver #2 below 0.8 Hz. This is due to the more severe steering correction of Eq. (28), meaning the vehicle is able to address the rollover threat in a more timely fashion. This similarity of results suggests that further analysis of third, fourth, etc., corrections is probably not necessary.

**4.3 Tire Lag Effects on Rollover Prevention.** When investigating dynamic effects that lead to vehicle wheel lift, tire lag could be an important contributor, as the delay in tire response may act in a manner to destabilize the roll dynamics of the vehicle. At certain speeds, the lag in tire force generation could amplify the roll effects of the suspension. This is especially true for corrective steering maneuvers, as the vehicle does not respond as quickly to changes in steering. Therefore, the simulations

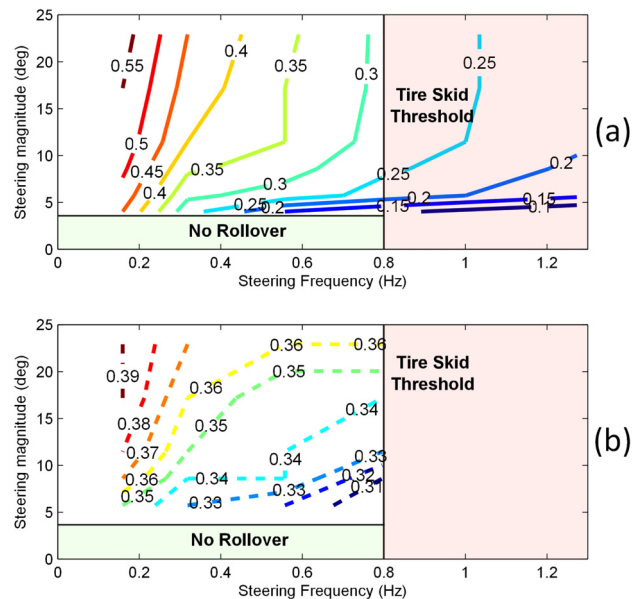


Fig. 14 Contour plot of minimum preview times (s) needed to prevent wheel lift for corrective steering #2 for (a) linear roll model and (b) CarSim. The Tire Skid Threshold indicates the steering frequencies above which skidding is likely to precede rollover. The No Rollover zone indicates where steering combinations did not induce wheel lift.

performed previously were repeated for the roll model with tire lag dynamics included. Tire relaxation values of 0.7 m and 0.23 m were used for the front and rear tires, respectively. These values were found by obtaining a range of standard values from Ref. [37] that were then tuned for the test vehicle.

Initial simulations showed that the infinite series of Eq. (19) in the previewed input coefficient,  $B_p$ , converged too slowly to be applied to the tire lag model. This was due to the fact that the modified terms in the state-space matrices had values several orders of magnitude larger than the matrices that did not include tire lag. Further testing showed that this also occurred for large preview times, even in the model without tire lag.

To address this problem, an alternate method [38] calculated the  $B_p$  matrix of Eq. (22) in discretized form with small time steps,  $\tau$ , added up to the preview time in the form

$$B_p = \sum_{m=0}^{n-1} (A_p^{n-1-m}) B \tau \quad (29)$$

where  $n = T/\tau$ . If the chosen time steps are small enough (a value of 0.001 s was used for this study), Euler approximation of  $A_p$  can be used such that Eq. (29) becomes

$$B_p = \sum_{m=0}^{n-1} [(I + A\tau)^{n-1-m}] B \tau \quad (30)$$

Equation (30) provides a more robust solution for the previewed input coefficient and allows the vehicle models with tire lag to be utilized. The disadvantage of this approach, however, is that it is more computationally expensive. For this reason, it was not used in the simulations presented previously.

The results of the rollover simulation, with tire lag dynamics included, showed that the preview time needed to prevent rollover only increased by approximately 0.01–0.02 s. This increase in preview time occurred for all steering combination inputs and for both corrective steering maneuvers. Therefore, the maximum required preview time for all conditions tested was 0.67 s, as opposed to 0.66 s when tire lag was not included.

Although this result suggests that tire lag effects are small and should be ignored, recall that the influence of tire lag on the dynamics of the vehicle is dependent on the longitudinal velocity. Tire lag effects become less important as the speed of the vehicle is increased. This is an intuitive relationship; as the tires revolve faster, they are able to generate lateral force more quickly from steering changes. Thus, at slower speeds, the effects of tire lag become more pronounced. To address the possibility that tire lag is a more important factor at lower speeds, simulations were performed to determine the preview times for various longitudinal velocities. Only the steering input that resulted in the maximum preview time (amplitude of  $-23$  deg; frequency of 0.2 Hz; corrective steering maneuver #1) was simulated. The preview times needed to prevent rollover were compared for the various longitudinal velocities for the roll model with and without tire lag as shown in Fig. 15.

As expected, slightly longer preview times were needed when considering the effects of tire lag at lower speeds. Speeds below 16 m/s saw an increase of approximately 0.04 s while speeds above 16 m/s saw an increase of only 0.01–0.02 s. Therefore, when considering preview horizons for rollover at high-speeds, it can be seen that the effect of tire lag on the necessary preview time is very small. For this particular steering combination, the effect of speed on the necessary preview time appears to be approximately linear, however, further testing would be necessary to confirm this relationship.

#### 4.4 Preview Times for Additional Vehicle Configuration.

Sections 4.1, 4.2, and 4.3 all examined simulations for a vehicle with a very high rollover propensity. Most vehicles, however, are less prone to the threat of wheel lift and should not need as much preview to mitigate the risk. To test this hypothesis, the corrective steering maneuver #1 simulations were repeated for the same vehicle (without tire lag), but with an artificially decreased CG height. Two additional variations of the truck simulated in Sec. 4.1 were tested, with modifications to the CG height as seen in Table 3. Here, we also aim to generalize the minimum preview curves by correlating each vehicle variation with its corresponding SSF [17]. The SSF is defined as

$$SSF = \frac{T_r}{2h} \quad (31)$$

The SSF values of the truck variations are also listed in Table 3. The SSF factor is considered here because it offers a simplified metric that does not depend on the vehicle's motion, but on its

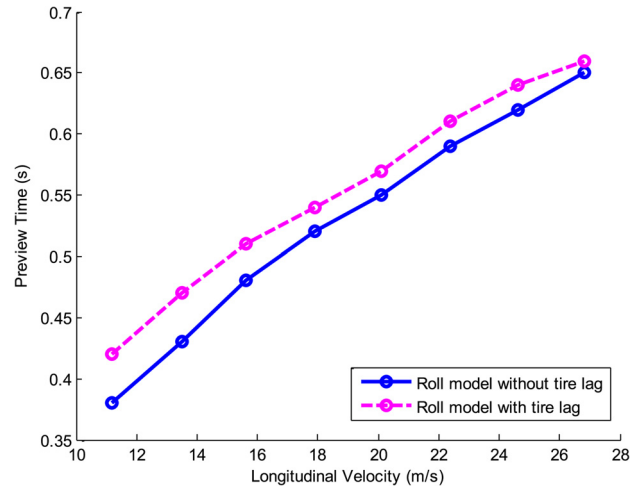


Fig. 15 Preview times needed to prevent wheel lift for varying longitudinal velocities ( $-23$  deg, 0.2 Hz steering combination)

Table 3 Variations to the CG height of the simulated 1989 GMC 2500 pick-up truck

Vehicle variation	$h$	$h_{sr}$	SSF
Original (#1)	1.234	0.781	0.654
#2	1.0	1.06	0.808
#3	0.7	0.75	1.155

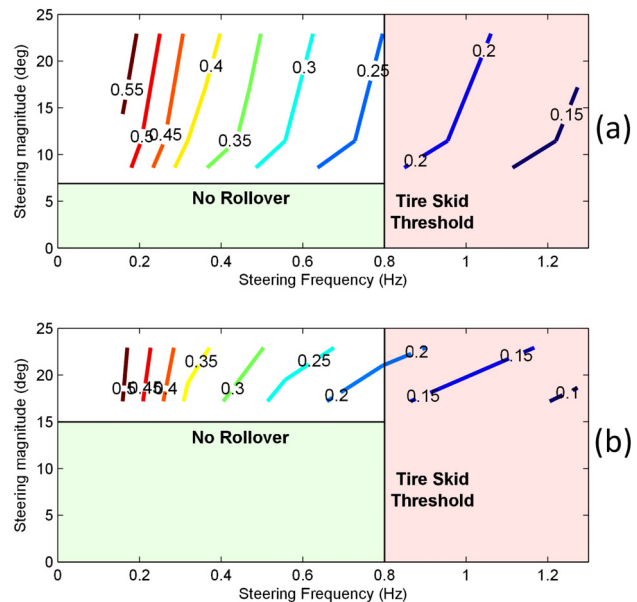
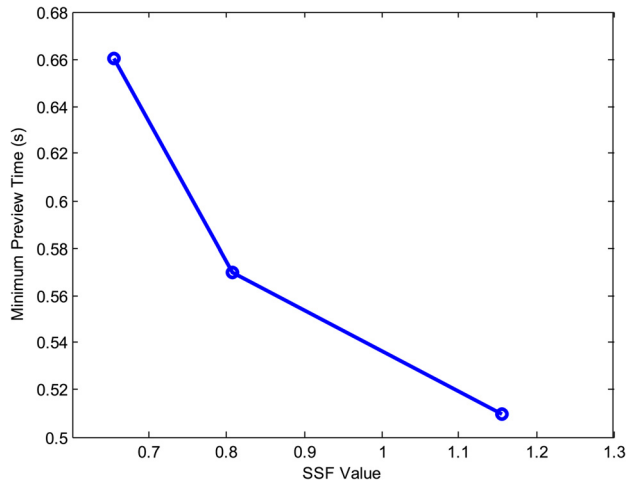


Fig. 16 Contour plot of minimum preview times (s) needed to prevent wheel lift for corrective steering #1 for (a) vehicle variation #2 and (b) vehicle variation #3. The Tire Skid Threshold indicates the steering frequencies above which skidding is likely to precede rollover. The No Rollover zone indicates where steering combinations did not induce wheel lift.

physical design. This would allow one to obtain information about the preview time even in the absence of a dynamic analysis.

The results of the corrective steering maneuver #1 simulations for the modified vehicle parameters are shown in Fig. 16. It can be seen that Fig. 16 exhibits the same trend as Fig. 8; however, less



**Fig. 17** Minimum preview times needed to prevent wheel lift for corrective steering #1 for each vehicle variation ( $-23$  deg,  $0.2$  Hz steering combination)

preview is needed for wheel lift prevention. As expected, Fig. 16 also exhibits an increase in the “safe zone” where no rollover occurs; as the vehicle’s rollover propensity decreases, lower steering magnitudes are not sufficient to induce wheel lift.

This trend can also be viewed from a more general perspective by looking at the relative SSF values of the three vehicle variations. Using the steering combination that requires the most preview ( $-23$  deg,  $0.16$  Hz steering input), Fig. 17 shows how the necessary minimum preview correlates with the SSF value of the vehicle. Although only three SSF values were simulated, the curve of Fig. 17 can be intuitively extrapolated such that asymptotic behavior is expected. Ultimately, as the SSF increases, there will be a point where the vehicle is so stable that no steering maneuver can induce untripped wheel lift, effectively resulting in zero necessary preview time. A similar plot to Fig. 17 could be constructed that looks at common SSF values and the necessary preview times

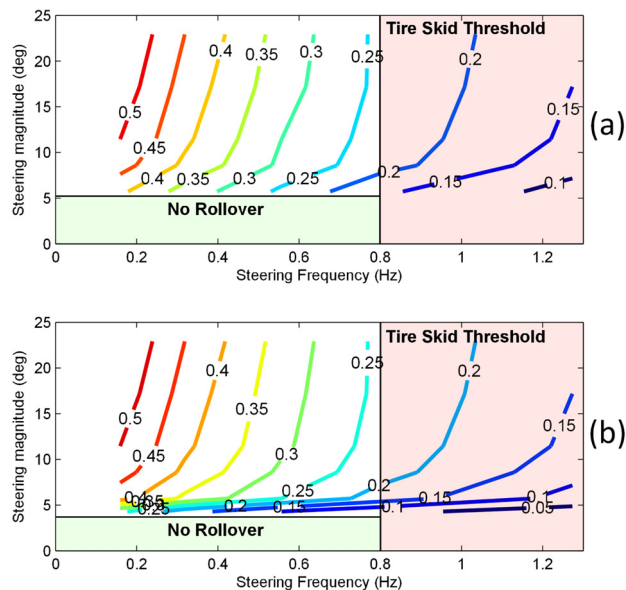


**Fig. 18** Contour plot of minimum preview times (s) needed to prevent wheel lift for corrective steering #1 for (a) a flat road ( $0$  deg bank angle) and (b) an intermediate slope ( $4$  deg bank angle). The Tire Skid Threshold indicates the steering frequencies above which skidding is likely to precede rollover. The No Rollover zone indicates where steering combinations did not induce wheel lift.

over the range of all steering combinations, serving as a guide for quickly choosing an estimate of the required preview time in intervention design.

**4.5 Bank Angle Effects on Preview Horizon.** Finally, this section examines how the preview horizon changes for different road superelevation values. The bank angle used in the simulations of Secs. 4.1–4.4 ( $8$  deg) was meant to create a “worst-case” situation for rollover. While this value is representative of the terrain seen on a sharp highway curve [35], it is relatively steep compared to the majority of driving conditions. Therefore, the corrective steering maneuver #1 simulations were repeated for two additional bank angle values: a flat road ( $0$  deg) and an intermediate slope ( $4$  deg) using the vehicle parameters of Table 2.

Figure 18 shows minimum preview horizons necessary for the different bank angles in the form of a contour plot. The results of Fig. 18 are intuitive and follow the trends seen in Secs. 4.1–4.4. The milder bank angles decrease the rollover propensity of the vehicle, resulting in slightly smaller minimum preview horizons. Additionally, an increase in the safe zone where no rollover occurs is seen for the flat road simulations. Overall, the ranges of preview times for the  $0$  deg slope ( $0.07$  s– $0.55$  s) and  $4$  deg slope ( $0.1$  s– $0.55$  s) are similar to the range seen in Sec. 4.1 for the  $8$  deg slope. On average, the minimum preview horizons decreased by  $0.06$  s for both the  $0$  deg slope and  $4$  deg slope when compared to the  $8$  deg slope.

## 5 Conclusions

In this study, the minimum preview time needed to predict and prevent vehicle wheel lift was determined. Results showed that preview horizons ranging from approximately  $0.1$  s– $0.7$  s ahead of the vehicle were sufficient to predict and prevent nearly all dynamics-induced rollovers under the conditions tested. These results looked at one particular worst-case vehicle scenario and configuration [26], as well as more modest vehicle configurations and bank angles with a decreased rollover propensity. As shown in Sec. 4.4, further changes to the vehicle parameters would likely result in different values of the necessary preview and can be correlated to the vehicle’s SSF value. Changes to the driving situation or intervention strategy (such as braking) would also likely result in changes in the minimum necessary preview. However, the methods presented in this study can readily accommodate these changes for the particular scenario or intervention being tested.

Determining an effective preview horizon for MPC-based approaches remains a challenging problem: the preview horizon must be long enough to predict future wheel lift, but short enough to allow real-time computation. While this study treats driver intervention as an open-loop control problem rather than a closed-loop MPC approach, the information about the necessary preview horizon for this work should be useful to aid in the design of either system.

## References

- [1] Department of Transportation, 2009, “2009 Traffic Safety Facts—Final Report,” U.S. Department of Transportation: National Highway Traffic Safety Board, Report No. DOT HS 811 402.
- [2] MacAdam, C. C., 1981, “Application of an Optimal Preview Control for Simulation of Closed-Loop Automobile Driving,” *IEEE Trans. Syst. Man Cybern.*, **11**(6), pp. 393–399.
- [3] Mammar, S., Glaser, S., and Netto, M., 2006, “Time to Line Crossing for Lane Departure Avoidance: A Theoretical Study and an Experimental Setting,” *IEEE Trans. Intell. Transp. Syst.*, **7**(2), pp. 226–241.
- [4] Sattel, T., and Brandt, T., 2008, “From Robotics to Automotive: Lane-Keeping and Collision Avoidance Based on Elastic Bands,” *Veh. Syst. Dyn.*, **46**(7), pp. 597–619.
- [5] Gray, A., Gao, Y., Hedrick, J. K., and Borrelli, F., 2013, “Robust Predictive Control for Semi-Autonomous Vehicles With an Uncertain Driver Model,” *IEEE Intelligent Vehicles Symposium*, Gold Coast, June 23–26, pp. 208–213.
- [6] Gray, A., Ali, M., Gao, Y., Hedrick, J. K., and Borrelli, F., 2012, “Integrated Threat Assessment and Control Design for Roadway Departure Avoidance,”

- 15th International IEEE Conference on Intelligent Transportation Systems (ITSC), Anchorage, AK, Sep. 16–19, pp. 1714–1719.
- [7] Anderson, S. J., Peters, S. C., Pilutti, T. E., and Iagnemma, K., 2010, “An Optimal-Control-Based Framework for Trajectory Planning, Threat Assessment, and Semi-Autonomous Control of Passenger Vehicles in Hazard Avoidance Scenarios,” *Int. J. Veh. Auton. Syst.*, **8**(2), pp. 190–216.
- [8] Falcone, P., Tufo, M., Borrelli, F., Asgari, J., and Tseng, H. E., 2007, “A Linear Time Varying Model Predictive Control Approach to the Integrated Vehicle Dynamics Control Problem in Autonomous Systems,” 46th IEEE Conference on Decision and Control, New Orleans, LA, Dec. 12–14, pp. 2980–2985.
- [9] Falcone, P., Borrelli, F., Asgari, J., Tseng, H., and Hrovat, D., 2007, “Predictive Active Steering Control for Autonomous Vehicle Systems,” *IEEE Trans. Control Syst. Technol.*, **15**(3), pp. 566–580.
- [10] Keviczky, T., Falcone, P., Borrelli, F., Asgari, J., and Hrovat, D., 2006, “Predictive Control Approach to Autonomous Vehicle Steering,” *American Control Conference*, Minneapolis, MN, June 14–16, pp. 4670–4675.
- [11] Brandt, T., Sattel, T., and Bohm, M., 2007, “Combining Haptic Human–Machine Interaction With Predictive Path Planning for Lane-Keeping and Collision Avoidance Systems,” IEEE Intelligent Vehicles Symposium, pp. 582–587.
- [12] Chen, B. C., and Peng, H., 2001, “Differential-Braking-Based Rollover Prevention for Sport Utility Vehicle With Human-in-the-Loop,” *Veh. Syst. Dyn.*, **36**(4–5), pp. 359–389.
- [13] Chen, B. C., and Peng, H., 2005, “Rollover Warning for Articulated Heavy Vehicles Based on a Time-to-Rollover Metric,” *ASME J. Dyn. Syst. Meas. Control*, **127**(3), pp. 406–414.
- [14] Yu, H., Guvenc, L., and Ozguner, U., 2008, “Heavy Duty Vehicle Rollover Detection and Active Roll Control,” *Veh. Syst. Dyn.*, **46**(6), pp. 451–470.
- [15] Schofield, B., and Hagglund, T., 2008, “Optimal Control Allocation in Vehicle Dynamics Control for Rollover Mitigation,” *American Control Conference*, Seattle, WA, June 11–13, pp. 3231–3236.
- [16] Carlson, C. R., and Gerdes, J. C., 2003, “Optimal Rollover Prevention With Steer by Wire and Differential Braking,” 2003 ASME Paper No. IMECE2003-41825.
- [17] Transportation Research Board, 2002, *The National Highway Traffic and Safety Administrations Rating System for Rollover Resistance*, National Academy Press, Washington, DC.
- [18] Dukkipati, R. V., Pang, J., Qatu, M. S., Sheng, G., and Shuguang, Z., 2008, *Road Vehicle Dynamics*, Society of Automotive Engineers, Warrendale, PA.
- [19] Ervin, R. D., and Guy, Y., 1986, “The Influence of Weights and Dimensions on the Stability and Control of Heavy-Duty Trucks in Canada Volume I,” The University of Michigan Transportation Research Institute, Ann Arbor, MI, Technical Report No. UMTRI-86-35/I.
- [20] Peters, S. C., and Iagnemma, K., 2009, “Stability Measurement of High-Speed Vehicles,” *Veh. Syst. Dyn.*, **47**(6), pp. 701–720.
- [21] Ryu, J., and Gerdes, J. C., 2004, “Integrating Inertial Sensors With GPS for Vehicle Dynamics Control,” *ASME J. Dyn. Syst. Meas. Control*, **126**(2), pp. 243–254.
- [22] Lapapong, S., and Brennan, S., 2010, “Terrain-Aware Rollover Prediction for Ground Vehicles Using the Zero-Moment Point Method,” *American Control Conference*, Baltimore, MD, June 30–July 2, pp. 1501–1507.
- [23] Lapapong, S., Brown, A. A., and Brennan, S. N., 2010, “Experimental Validation of Terrain-Aware Rollover Prediction for Ground Vehicles Using the Zero-Moment Point Method,” 10th International Symposium on Advanced Vehicle Control (AVEC2010), Vol. 2, Longsborough, UK, pp. 1233–1237.
- [24] Lapapong, S., 2010, “Vehicle Rollover Prediction for Banked Surfaces,” Ph.D. dissertation, The Pennsylvania State University, University Park, PA.
- [25] Lapapong, S., and Brennan, S., 2011, “A Novel Comparative Approach to Evaluate Vehicle Rollover Propensity,” 2011 IAVSD, Manchester, UK.
- [26] Lapapong, S., Brown, A., Swanson, K., and Brennan, S., 2012, “Zero-Moment Point Determination of Worst Case Maneuvers Leading to Vehicle Wheel Lift,” *Veh. Syst. Dyn.*, **50**(Suppl. 1), pp. 191–214.
- [27] Sardain, P., and Bessonnet, G., 2004, “Forces Acting on a Biped Robot. Center of Pressure—Zero Moment Point,” *IEEE Trans. Syst. Man Cybern. A*, **34**(5), pp. 630–637.
- [28] Vukobratovic, M., and Juricic, D., 1968, “Contribution to the Synthesis of Biped Gait,” Proceedings of IFAC Symposium on Technical and Biological Problem on Control, Erevan, USSR, pp. 1–6.
- [29] Mammari, S., Baghdassarian, V. B., and Nouveliere, L., 1999, “Speed Scheduled Lateral Vehicle Control,” *International Conference on Intelligent Transportation Systems*, Tokyo, Japan, pp. 80–85.
- [30] Shim, T., and Ghihe, C., 2007, “Understanding the Limitations of Different Vehicle Models for Roll Dynamics Studies,” *Veh. Syst. Dyn.*, **45**(3), pp. 191–216.
- [31] Society of Automotive Engineers, 1976, *Surface Vehicle Recommended Practice*, Society of Automotive Engineers, Warrendale, PA.
- [32] Levinson, J., Montemerlo, M., and Thrun, S., 2007, “Map-Based Precision Vehicle Localization in Urban Environments,” *Robotics: Science and Systems*, MIT Press, Cambridge.
- [33] Eisele, D. D., and Peng, H., 2000, “Vehicle Dynamics Control With Rollover Prevention for Articulated Heavy Trucks,” 5th International Symposium on Advanced Vehicle Control: AVEC2000, Ann Arbor, MI.
- [34] Bay, J. S., 1999, *Fundamentals of Linear State Space Systems*, McGraw-Hill, Boston.
- [35] American Association of State Highway and Transportation Officials, 2011, *A Policy on Geometric Design of Highways and Streets*, American Association of State Highway and Transportation Officials, Washington, DC.
- [36] Department of Transportation, 2013, *Laboratory Test Procedure for Dynamic Rollover: The Fishhook Maneuver Test Procedure*, U.S. Department of Transportation: National Highway Traffic Safety Administration, Washington, DC.
- [37] Dixon, J., 1996, *Tires, Suspension, and Handling*, 2nd ed., Society of Automotive Engineers, Warrendale, PA.
- [38] Kulakowski, B., Gardner, J., and Shearer, J., 2007, *Dynamic Modeling and Control of Engineering Systems*, 3rd ed., Cambridge University Press, New York.